Materials Science and Engineering, 30 (1977) 99 - 111
© Elsevier Sequoia S.A., Lausanne — Printed in the Netherlands

22

A Model for Elastic Precursor Waves in the Shock Loading of Polycrystalline Metals

MARC A. MEYERS

Dept. of Metallurgical Engineering, South Dakota School of Mines and Technology, Rapid City, South Dakota 57701 (U.S.A.)

(Received March 28, 1977)

SUMMARY

When materials are shock loaded in a certain range of pressures, the shock wave is preceded by an elastic wave. This elastic precursor wave can undergo relaxation and changes in amplitude and rise time as it traverses the material. Both the wave attenuation and relaxation have been interpreted in the past in terms of dislocation dynamics. This study addresses itself to the wave rise times. The different rise times reported in the literature are reviewed and some trends are identified, namely, that (a) single crystals have usually shorter rise times than polycrystals, (b) rise times increase with transit distance, and (c) in polycrystalline metals rise times are affected by grain size and texture. A model for the rise times of elastic waves in polycrystalline metals is developed. It incorporates the following parameters: anisotropy of wave velocity, scattering by grain boundaries, mode conversion and deflection due to anisotropy of adjacent grains, dislocation effects, and intrinsic wave rise time. The results predicted by the model are compared to experimental results by Jones and Holland [26] for three different grain sizes and good agreement is found. Also, the model is consistent with other results reported in the literature.

1. INTRODUCTION

Shock waves in metals are usually investigated under experimental conditions resulting in a state of uniaxial strain. This can be accomplished, among other ways, by the impact of a plane driver plate on a parallel plane target or by the direct detonation of explosive in contact with the material. At low peak amplitudes only an elastic wave is generated. If the amplitude of the wave becomes higher than the Hugonot elastic limit of the target material, the wave decomposes into an elastic precursor and a trailing plastic (shock) wave. Since the velocity of the plastic wave increases with peak pressure, there is a certain "overdrive" stress, above which the plastic wave "gulps" the elastic precursor wave. The elastic precursor wave has attracted considerable interest in the past few years, since it is possible to obtain information on dislocation dynamics from it. It is needless to say that dislocation dynamical considerations are of tantamount importance to the understanding of the substructure formation in high-velocity deformation. Taylor and Rice [1] first observed the decay of the elastic precursor amplitude with depth of penetration into the target; Taylor [2] later explained it successfully in terms of the Johnson–Gilman [3] expression for dislocation velocity. Another feature observed is yield point formation [1, 4, 5] and, consequently, stress relaxation behind the elastic precursor; Barker, Butcher and Karnes [4] attributed it to dislocation effects predicted by the Johnson–Gilman model. Kelly and Gillis [6] showed that thermal activation models (*e.g.*, ref. 7) for dislocation dynamics could explain the observed decay behavior as well as the Johnson–Gilman model. Johnson [8] extended the Taylor [2] interpretation of precursor decay to polycrystalline metals. Rohde [9] studied the precursor decay in iron shock-loaded at temperatures ranging from 76 to 573 K and found that the data did not satisfy entirely any of the following models: the Johnson–Gilman model [3], the activation energy model [7], or the linear damping model [10]. The work has been reviewed extensively [11 - 14].

2. STATEMENT OF THE PROBLEM

While precursor attenuation and relaxation have stimulated considerable work, its rate of rise has only received scant attention in the past. To the author's knowledge, Arvidsson *et al.* [5] were the only ones to investigate systematically the change in precursor rise times and suggest a mechanism. However, if one carefully analyzes the data available in the literature, one can notice substantial differences in the rise times. These variations are not random, and there are some definite trends that will be described below. Most of the measurements reported were made using quartz gages having dimensions well above the grain sizes. Whenever a different technique was used, it will be specified. Where no mention is made, the use of quartz gages is implicit. The following trends are observed in the literature:

(a) Single crystals have a tendency to exhibit shorter elastic precursor rise times than polycrystals. Jones and Mote [16] shock-loaded copper crystals (thickness around 5 mm) with orientations [100], [110], and [111] parallel to the shock direction and found rise times of the order 0.010 μs. An annealed polycrystalline copper sample (average grain diameter of 4.5 mm) with a thickness of 3.91 mm exhibited a sloping precursor with a rise time of 0.1 μs. It is worth noticing, however, that the short rise times were not observed in the pre-strained Cu single crystals. Jones and Mote [16] attributed the differences to dislocation effects. Barker and Hollenbach [42] found shock-like elastic fronts in synthetic Al_2O_3 (sapphire) single crystals, using interferometer instrumentation techniques. Gupta *et al.* [18] found, in 18 out of 20 experiments with LiF single crystals, that the rise times of the elastic precursor waves matched the tilt of the flyer plate target at the instant of impact. That is, the rise times could, in 18 of 20 experiments, be totally accounted for by the tilt. This is equivalent to say that the rise times in LiF are very short. Dick *et al.* [19] present plots where the short rise times can be seen (~0.01 μs); the only exception is an experiment at a pressure below the dynamic yield stress.

Single-crystal beryllium was shocked by Pope and Stevens [20] and Pope and Johnson [21]; shocking was done by plate impact and along the *a* and *c* axes, as well as off-axis directions. In all cases the rise times of the elastic waves were of the order of a few nanoseconds. On the other hand, polycrystalline beryllium tended to exhibit much higher rise times [22, 23]. Longer rise times have also been observed in a variety of other polycrystalline materials. For example, Grine [24] found increasing precursor rise times with the increase in transit distance of a shock wave through polycrystalline granite. At 127 mm from the surface, the rise time had increased from zero (at surface) to around 1 μs.

Barker *et al.* [4] found some interesting differences upon shock loading polycrystalline aluminum (average grain diameter of 1 mm). The rise times observed by means of quartz gages were about 0.08 μs, while laser interferometry provided durations of about 0.015 μs. They said that the difference could be explained by the difference between the active diameters of the quartz gage (12.7 mm) and of the interferometer light spot (0.1 mm). Also, the interferometer results suffered from non-repeatability and Barker *et al.* [4] suggested that it could be due either to experimental conditions or intrinsic characteristics of the aluminum. Gillis *et al.* [25], upon shock-loading polycrystalline tantalum, found a rise time of 0.05 μs after making necessary corrections for projectile tilt. Shock-loaded iron [26] showed elastic rise times varying between 0.028 and 0.088 μs; Rohde [9] found a rise time of around 0.12 μs for iron shock-loaded at room temperature.

(b) Rise times increase with transit distances inside the metal. Recently, Arvidsson *et al.* [15] have shown that, for polycrystalline aluminum, the rise time increases with penetration within the target. Grine [24], as mentioned earlier, observed the same effect in granite.

(c) In polycrystalline metals, rise times are affected by grain size and texture. Jones and Holland [26] found substantial variations in the elastic rise times of shock-loaded iron. They showed a tendency to increase with grain size, all other parameters being maintained constant. Stevens and Pope [23] submitted polycrystalline beryllium samples of four different textures to plate impact experiments. They found that, as the texture in-

creased, the rise time of the elastic precursor decreased. The articles above, because of their relevance to the present study, will be discussed later in greater detail.

While differences in the rise times of elastic waves exist, and in spite of the fact that there are — as shown above — some definite tendencies in these differences, there are only short, speculatory statements on them in the literature (with the exception of Arvidsson *et al.* [15]). The major concern of previous investigations was usually precursor attenuation and relaxation. Jones and Holland [26] attributed the differences to impedance mismatches between the adjacent grains, resulting in reverberations of the disturbance. Jones and Mote [16] interpreted the differences between copper single crystals and polycrystals as being due to lower initial dislocation density in the former. Gillis *et al.* [25] explained the finite rise time in polycrystalline tantalum as being due to the pre-existing dislocations. Stevens and Pope [23] attributed the ramping rise time in untextured polycrystalline beryllium to unrelaxed thermal stresses. In textured beryllium, the crystallographic alignment would permit relaxation of the microstresses and the precursor rise time would decrease. Arvidsson *et al.* [15] concluded that the increase in elastic rise times with distance was due to viscosity effects.

It can be seen from the above that there is no general agreement on the reasons for a finite rise time of elastic precursor waves. For this reason it was thought worthwhile to analyze the possible causes for this effect and to present a model consistent with the results reported in the literature and described above.

3. MODEL FOR RISE TIMES OF ELASTIC PRECURSOR WAVE IN POLYCRYSTALLINE METALS

An elastic precursor wave is schematically represented in Fig. 1. It is, of course, recognized that the uniaxial strain generates a triaxial state of stress at the wave [14]. However, for reasons of simplicity only the normal component in the wave propagation direction is considered. σ and $\Delta\sigma$ are the peak amplitude and stress decay, respectively. They have been interpreted successfully in terms of dislocation dynamics [2 - 14]. Δt is the rise

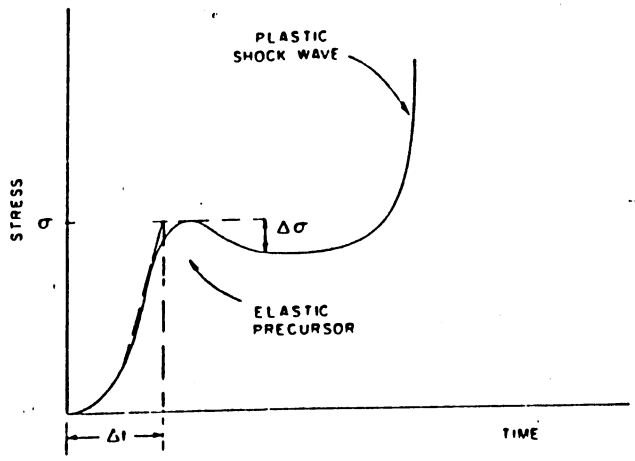

Fig. 1. Schematic representation of elastic precursor wave.

time of the elastic wave. A complete model for the elastic precursor wave would necessarily have to incorporate the σ decay and $\Delta\sigma$. These parts will be intentionally left out and only the precursor rise will be analyzed. In polycrystalline metals there is a series of effects that may affect the rise time of the wave. Assuming a perfectly parallel projectile-target impact, or a perfectly simultaneous explosive detonation at the target surface, the most important effects capable of introducing irregularities into the elastic precursor waves are:

(a) Velocity anisotropy. The wave velocity is a function of the direction of propagation in a crystal. For this reason the mean velocity of a wave traveling along a straight path will depend upon the orientation of the grains. Consequently, waves traveling along straight paths where different crystallographic densities occur will have different mean velocities. A similar treatment was previously presented by Meyers and Carvalho [27] for shock waves.

(b) Scattering by grain boundaries. Grain boundaries should act as barriers to a propagating elastic wave, because they are two-dimensional inhomogeneities, with atomic arrangement and density different from the matrix.

(c) Wave deflections at grain boundaries due to anisotropy of adjacent grains. Adjacent grains with different orientations may be visualized as different materials due to elastic anisotropy. So, both reflection and refraction take place at the grain boundaries due to the

boundary conditions of constancy in pressure and strain compatibility at the interface [28]. Refraction will change the orientation of the transmitted wave, resulting in a non-linear path.

(d) Scattering due to mode conversion (from longitudinal to shear waves, and *vice-versa*), when a wave traverses different grains. This is related to item (c) and will be discussed later. Delaying effects are introduced because shear waves propagate at velocities much lower than longitudinal waves.

(e) Initial rise time of wave at instant of impact. The projectile undergoes deceleration upon impacting the target. The elastic precursor wave has an initial rise time that is different from zero.

(f) Dislocation dynamical effects. Finite rise times have been attributed to these effects.

Of the above effects, only (e) and (f) increase the actual rise time of the wave. The other effects tend to produce an irregular, wavy wave front. A gage with an active area larger than the material grain size will present a wave profile that incorporates both the actual rise time of the wave and irregularities producing waviness in the elastic front. Such is the case of quartz and manganin gages. On the other hand, laser interferometry should give a more realistic profile of the *actual* rise times. A model that would explain the rise times observed in quartz gages should incorporate time delays due to effects(a) to (f) above. So:

$$\Delta t = \Delta t_a + \Delta t_b + \Delta t_c + \Delta t_d + \Delta t_e + \Delta t_f \qquad (1)$$

where the subscripts refer to the letter of the corresponding effect in the above listing. The various time delays will be estimated and their sum will be compared with the results obtained by Jones and Holland [26]. This work was chosen because it allows comparison when one parameter — the average grain diameter — was varied, the others remaining constant. Also, Jones and Holland [26] used a disc-shaped quartz transducer with an active diameter of 21.75 mm, when the grain sizes were 70×10^{-3} mm or smaller. Iron samples with thickness of 19.05 mm and average grain diameters ranging from 9 to 70.3 μm were used by them.

3.1 Velocity anisotropy

The elastic wave velocities along straight paths, as well as the probabilities of the different paths, can be calculated. From this combined information Δt_a can be estimated. This calculation procedure, applied to Jones and Holland's [26] conditions, is shown next.

The longitudinal components of elastic waves along the three crystallographic orientations ⟨100⟩, ⟨110⟩, and ⟨111⟩ can be calculated in terms of the elastic stiffnesses C_{11}, C_{12}, C_{44} and the material density; expressions are given by Ghatak and Kothary [29] (there are misprints in the original version). The correct forms of the expressions are:

$$U_{\langle 100\rangle} = \sqrt{\frac{C_{11}}{\rho}} \qquad (2)$$

$$U_{\langle 110\rangle} = \sqrt{\frac{C_{11} + C_{12} + 2C_{44}}{2\rho}} \qquad (3)$$

$$U_{\langle 111\rangle} = \sqrt{\frac{C_{11} + 2C_{12} + 4C_{44}}{3\rho}} \qquad (4)$$

For iron, the values of the elastic stiffnesses are, at 300 K [30]:

C_{11} = 243.1 GPa

C_{12} = 138.1 GPa

C_{44} = 121.9 GPa.

The density of iron is 7.860 at 300 K, so:

$U_{\langle 100\rangle} = 5.56 \times 10^6$ mm/s

$U_{\langle 110\rangle} = 6.31 \times 10^6$ mm/s

$U_{\langle 111\rangle} = 6.53 \times 10^6$ mm/s.

An elastic wave profile can be estimated at any position inside the polycrystalline iron sample knowing the grain size and texture. The calculations can be conducted in various degrees of rigorousness. An approximate profile that does not require extensive mathematical manipulation can be produced by making some simplifying assumptions and specifying some parameters:

(a) All grains are cubes with sides, L, as shown in Fig. 2. For the three grain sizes considered, cubes with the following sides L will be assumed: 9, 34, and 70.3 μm. The longitudinal elastic wave front is horizontal and travels from top to bottom.

(b) It is assumed that there are only three vertical orientations for the grains: ⟨100⟩,

TABLE 1
Number of grains and transit times for the three different grain sizes

Cubic grain size, L (μm)	Number of grains, n	Transit time per grain	
		grain type 1, t_1 (μs x 10^{-3})	grain type 2, t_2 (μs x 10^{-3})
9	2116	1.62	1.40
34	560	6.12	5.30
70.3	270	12.64	10.95

⟨110⟩ and ⟨111⟩. These are the sole orientations along which purely longitudinal waves exist [29]. It will also be assumed that the material exhibits the least possible texturing. To make the two above assumptions compatible the grains have to be present in proportion to the multiplicity factor of their vertical orientation: these are 6, 12 and 8 for the ⟨100⟩, ⟨110⟩ and ⟨111⟩ orientations, respectively. Consequently, the probabilities for the orientation of each grain are:

$p_{\langle 100\rangle} = 0.461$

$p_{\langle 110\rangle} = 0.231$

$p_{\langle 111\rangle} = 0.308.$

(c) Since the velocities of the waves along the ⟨110⟩ and ⟨111⟩ orientations are very close, an average of the two is taken and their probabilities added up. This simplification introduces enormous reductions in the computer processing times. So, two orientations, ⟨100⟩, and ⟨110⟩ + ⟨111⟩, are considered. They are coded 1 and 2, respectively, in the expressions that follow.

(d) The wave profile will be evaluated after it penetrated 19.05 mm into the iron sample.

Table 1 shows the number of grains and transit times for the three different grain sizes. In order to obtain the probability distribution function of the transit times after a penetration of 19.05 mm has been reached, one can state the problem statistically as: what is the probability distribution function of n indistinguishable events 1 and 2, with probabilities p_1 and p_2 and values t_1 and t_2? The number of cubes that the wave would have to traverse, in its vertical path, is n; p_1 and p_2 are 0.461 to 0.539, respectively, and are the probabilities previously referred to; t_1 and t_2 are the transit times for the cubes of two orientations. They are obtained by:

$$t_1 = \frac{L}{U_1} \text{ and } t_2 = \frac{L}{U_2} \tag{5}$$

where L has three possible values (Table 1). One has to determine the number of possible configurations, C, of n_1 events of type 1 and n_2 events of type 2 ($n_1 + n_2 = n$):

$$C = \frac{n!}{n_1!\, n_2!} \tag{6}$$

The probability, p, of each outcome is:

$$p = p_1^{n_1} \times p_2^{n_2} \tag{7}$$

The total probability, P, of each outcome is:

$$P = pC. \tag{8}$$

One should expect that:

$$\Sigma P = 1. \tag{9}$$

The transit time, T, of each outcome is:

$$T = n_1 t_1 + n_2 t_2. \tag{10}$$

A plot of T *vs.* P provides the distribution of transit times at a penetration distance of 19.05 mm.

Expressions (6), (7), (8) and (10) were fed into an IBM 1130 computer in the form of an especially prepared program. Due to the computer limitations — it only operates with numbers ranging from 10^{38} to 10^{38} — the logarithmic form of eqn. (8) was used and values of P lower than 10^{-38} were assumed zero. This only produced very small errors, as shown in Table 2. The summation of total probabilities should be 1, (eqn. 9) if no value of P was neglected. A plotter expressed graphically the computer results.

Figures 3, 4 and 5 show the T *vs.* P plots for the grain sizes of 70.3, 34, and 9 μm, respectively. The values of P were grouped in the same time intervals of 2.5×10^{-3} μs in the three Figures. Therefore, the three distri-

TABLE 2

Summation of total probabilities and standard deviations of time

L (μm)	ΣP	Std. deviation (μs)	Δt_a (μs)
9	0.983 9	0.005 69	0.022 76
34	0.998 4	0.010 02	0.040 08
70.3	0.999 5	0.014 25	0.057 00

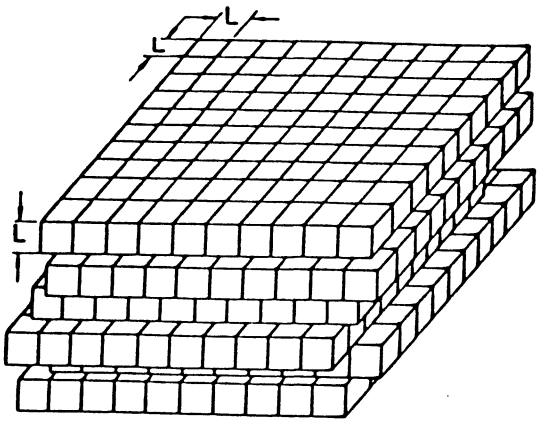

Figure 2. Simplified configuration for the grains.

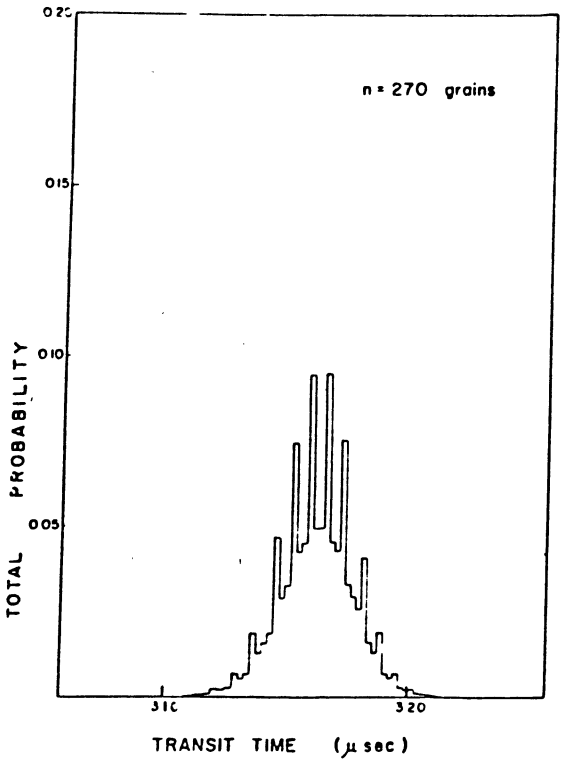

Figure 3. Distribution of transit times due to velocity anisotropy of the wave, after penetration of 19.05 mm into sample with grain size of 70.3 μm, as obtained from computer calculations.

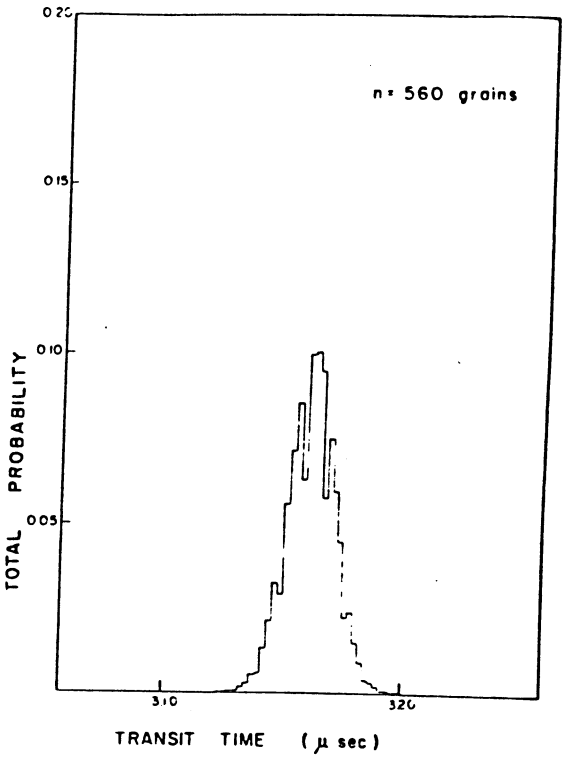

Figure 4. Distribution of transit times due to velocity anisotropy of the wave, after penetration of 19.05 mm into sample with grain size of 34 μm, as obtained from computer calculations.

bution functions can be directly compared. Their mean is the same: 3.16 μs. However, as the grain size increases (and, consequently, the number of grains decreases) the distribution broadens out. The standard deviations for the three distributions are given in Table 2. One can infer, from the plots of Figs. 3, 4 and 5, that the elastic wave progresses into the material not as a planar front, but with irregularities that become increasingly pronounced; therefore, the "wavy wave" name.

Four standard deviations were thought to be a good measure of Δt_a because around 95% (if one assumes a normal distribution) of the transit times are within this interval in the distributions of Figs. 3 - 5. The values are presented in Table 2.

3.2 Scattering by grain boundaries

Grain boundaries can be visualized, for the purpose of wave propagation as inhomogeneities having a few atomic layers of thickness. Because they scatter the wave, they should contribute to its attenuation. Their effect on the rise time, Δt_b, can be best inferred from the work of Stevens and Pope [23]. As

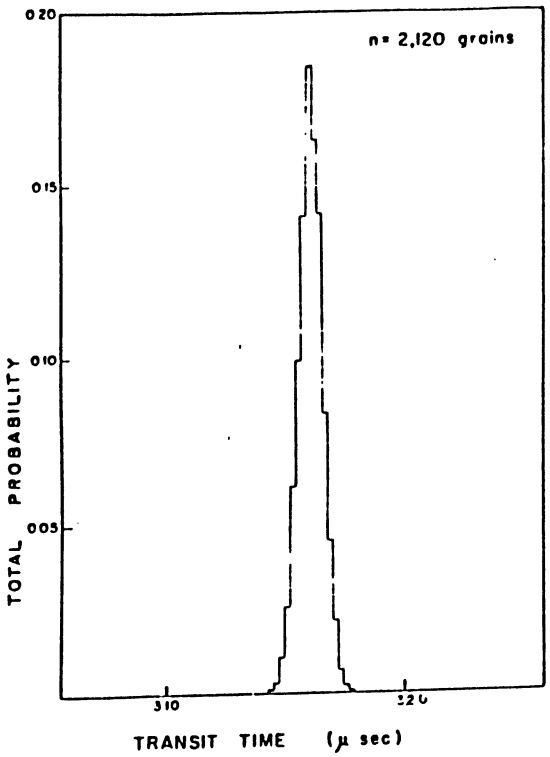

Fig. 5. Distribution of transit times due to velocity anisotropy of the wave, after penetration of 19.05 mm into sample with grain size of 9 μm, as obtained from computer calculations.

described earlier, they shock-loaded polycrystalline beryllium samples with different basal plane texture factors (1 R - 8 R, where R is the basal plane density for the random sample). All samples had grains not too different from equiaxial, and of approximately the same size. However, changes in pulse durations were observed; these changes cannot be due to grain-boundary scattering. Moreover, the 5 R and 8 R samples had an elastic precursor rise time of 4×10^{-3} μs. So, the times rises introduced by the grain boundaries should be lower than 4×10^{-3} μs. This number could be taken as a rough estimate of Δt_b for iron, since actual calculations could be extremely complex.

3.3 Deflections at grain boundaries due to anisotropy of adjacent grains

The elastic wave in parallel plate impact experiments is initially entirely longitudinal and travels in a direction perpendicular to the impact surface. However, as it encounters boundaries of different grains, it is reflected and refracted, and generates reflected and

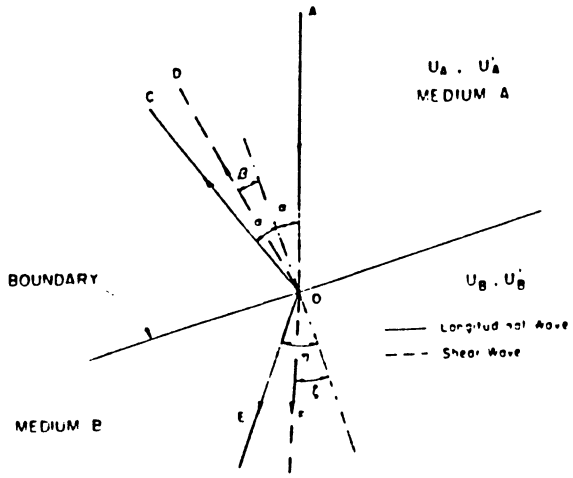

Fig. 6. Reflected and refracted waves when longitudinal wave OA encounters boundary between media A and B with different wave impedances.

refracted shear components. This is due to the fact that different grain orientations have different acoustic impedances or resistances (defined as the product of the wave velocity by the density).

Again, some simplifying assumptions are necessary in order to determine the time rise, Δt_c. Figure 6 shows a longitudinal wave, AO, inciding on a boundary separating materials with different acoustic impedances. It generates a transmitted longitudinal wave, OE, and shear wave, OF, and a reflected longitudinal wave, OC, and shear wave, OD. So, the wave OA generates four waves. The longitudinal and shear velocities are indicated by U and U', respectively. The angles and amplitudes depend upon the acoustic impedances of the two media, the wave velocities, the initial incidence angle α, and the amplitude of AO. The calculations are described by Kolsky [31], Rinehart [28] and Wasley [41]. In the following calculations the iron sample will be assumed, as in Section 3.1, to be composed of grains with two orientations: ⟨100⟩ and ⟨110⟩ + ⟨111⟩. For simplicity, these grains will be assumed isotropic (but with different acoustic impedances) so that longitudinal and shear waves can travel in them along any direction. Actually, perfectly longitudinal and shear waves only propagate along certain orientations within a crystal [32]. Along all other orientations, only quasi-longitudinal and quasi-shear waves can exist [33]. The angles of the transmitted and reflected waves

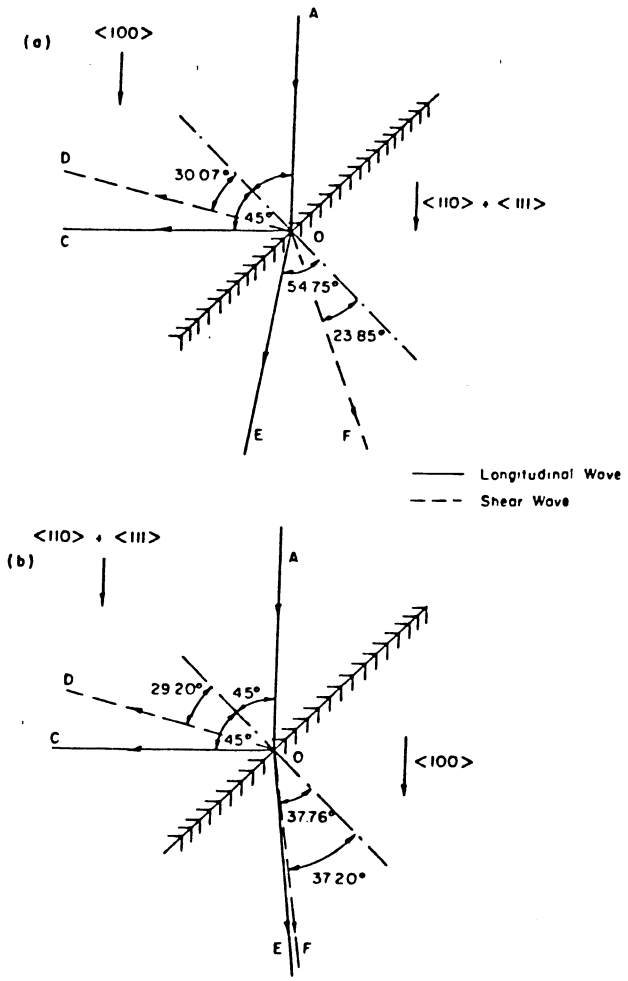

Fig. 7. Reflected and refracted waves when longitudinal wave OA encounters boundary at 45°. (a) Wave going from ⟨100⟩ into ⟨110⟩ + ⟨111⟩. (b) Wave going from ⟨110⟩ + ⟨111⟩ into ⟨100⟩.

with the boundary normal are given by [28, 31]:

$$\frac{\sin\alpha}{U_A} = \frac{\sin\beta}{U'_A} = \frac{\sin\eta}{U_B} = \frac{\sin\xi}{U'_B} \qquad (11)$$

If the grain configuration of Fig. 2 were assumed, all angles would be equal to 90° and the wave would maintain a straight path. However, this approximation cannot be made here. The grains will be assumed to the polyhedra of equal size; Rhines *et al.* [34] describe the ideal grain as a tetrakaidecahedron. For such a situation, a longitudinal wave will intercept boundaries at angles, α, varying from 0 to 90°. It can be clearly seen that the transmitted longitudinal wave will continuously be deflected from its straight path. These deflections depend on the angle, α. They vary from 0 (for $\alpha = 0$) to a maximum value, for $\alpha = 90°$. Therefore, the path length of the longitudinal wave will be increased from its minimum value of 19.5 mm. The complications of a rigorous calculation are enormous, and it suffices in this estimate to consider average deflections. An average α angle of 45° is assumed, and two situations are considered: the wave crossing the boundary from ⟨100⟩ to ⟨110⟩ + ⟨111⟩ and the wave going from ⟨110⟩ + ⟨111⟩ to ⟨100⟩. The results are presented in Fig. 7(a) and (b), respectively. In Fig. 7(a) the longitudinal wave is deflected to the left by 9.75°; in Fig. 7(b), it is deflected by 7.24° to the right. The transmitted shear wave and reflected waves will be treated in Section 3.4 and are of no concern here.

At this point a new simplifying assumption is introduced. It is assumed that an average wave is successively deflected to right and left, so that the wave follows, macroscopically, a linear path. The microscopic deflections (having the mean amplitude equal to the mean grain diameter) to right and left are assumed to be the same and equal to the average of the deflections shown in Fig. 7. So, the mean deflection at each boundary is 8.5°. If the path is assumed to be macroscopically linear and vertical, this corresponds, microscopically, to a wave fluctuation of 4.25° around a vertical straight line. The calculation of this increased path length is straightforward. If the straight path length is L, then:

$$L_1 = \frac{L}{\cos 4.25°}$$

For Jones and Holland's [26] experimental situation, L is 19.05 mm and L_1 would be 19.103 mm. So, there is a mean path increase of 0.053 mm associated with deflections of the longitudinal waves at grain boundaries due to grain anisotropy. Non-linearity of the wave paths will increase the waviness of the wave beyond the waviness strictly due to anisotropy of velocities. The minimum path length being 19.05 mm and the mean 19.103 mm, there will also be portions of the wave that will have a longer path length. An interval of twice the 0.053 mm is a first estimate of the range of path lengths encompassing the majority of situations. By dividing the value of 0.106 mm by the mean velocity of the wave, one obtains the time of 0.017 6 μs. This time represents the difference in wave

TABLE 3

Relative amplitudes (amplitude of wave divided by amplitude of incident wave OA) of transmitted and reflected waves

Wave	From ⟨100⟩ to ⟨110⟩ + ⟨111⟩	From ⟨110⟩ + ⟨111⟩ to ⟨100⟩
OC/OA	0.41	−0.30
OD/OA	0.27	0.20
OE/OA	1.17	1.22
OF/OA	−0.30	0.09

arrival times at the quartz gage due to deflections at grain boundaries. It is, therefore, an estimate of Δt_c. So, $\Delta t_c = 0.017\,6\ \mu s$. This value should be the same for all grain sizes.

3.4 Scattering due to mode conversion (from longitudinal to shear waves, and vice versa) at grain boundaries

Figure 6 shows how a longitudinal wave generates two shear and two longitudinal waves. The orientations of these waves are shown in Fig. 7. The assumptions made in Section 3.3 are maintained here. The orientations of the transmitted and reflected shear waves are obtained by means of eqn. (11), using the shear wave velocities calculated from Ghatak and Kothari [29]. The following velocities were obtained:

$U'_{\langle 100\rangle} = 3.94 \times 10^6$ mm/s

$U'_{\langle 110\rangle} = 3.26 \times 10^6$ mm/s (average of two modes)

$U'_{\langle 111\rangle} = 3.10 \times 10^6$ mm/s.

As with the longitudinal velocities, the orientations ⟨110⟩ and ⟨111⟩ are grouped and their average shear velocity is taken. So:

$U'_1 = 3.94 \times 10^6$ mm/s

$U'_2 = 3.18 \times 10^6$ mm/s.

The amplitudes of the reflected and transmitted waves have to be calculated in order to verify whether they can affect the rise time of the elastic precursor waves. The amplitudes can be calculated [28, 31, 41], and their ratio to the amplitude of the incident wave is given in Table 3, for a 45° incidence. The minus sign for the longitudinal wave means that it is tensile; for the shear wave, it represents particle displacement in a direction opposite to the direction providing a positive sign. It can be seen that the refracted longitudinal wave carries most of the energy for both situations. In one case the reflected longitudinal wave is tensile and in the other it is positive; having approximately the same relative amplitude and propagating at approximately 90° to the primary propagation direction, they will, in the average, annihilate each other. Because of the assumptions, or the nature of the equations used, the energy is apparently not conserved at the boundary. So the relative values of the ratios and not their absolute values should be considered. Of course, the ratios change with the angle of incidence, α; but, as in the preceding Section, 45° is taken as a good overall value. Because their velocity is only around 2/3 of the longitudinal waves, the shear waves will trail far behind the elastic wave front and will therefore not affect the rise time of the wave. One may argue that OF (Fig. 7) might reconvert to a longitudinal wave in the next grain boundary. The scattering of shear waves at grain boundaries is similar to the one by longitudinal waves (Fig. 6). But the amplitude of a longitudinal wave resulting from a transmitted shear wave would be negligible. An idea of its relative amplitude can be obtained by the square of the relative amplitude of OF. The reflected shear and longitudinal waves are also of no great concern since they are moving away from the macroscopic propagation direction. Δt_D can be taken as zero. Papadakis [35] presents an analysis of the effects of polycrystallinity on ultrasonic waves and says that attenuation is determined almost entirely by grain scattering. It is interesting that, to the author's knowledge, grain scattering has not at all been involved in the interpretation of the attenuation of elastic precursor waves in polycrystalline metals. From the above analysis one can see that polycrystallinity is responsible for wave scattering and, consequently, attenuation, but that the rise time should not be affected because of the lower amplitudes and velocities of reflected and refracted shear waves.

3.5 Initial rise time of wave at instant of impact

The elastic wave has an intrinsic rise time due to the finite velocity of the projectile (in

the case of impact) or the rate of pressure increase due to detonation (in the case of shocking by direct contact with the explosive). This intrinsic time rise is due to the fact that the rate of application of pressure has a finite value. After the elastic pulse penetrates into the metal, its rise time would steadily increase if the higher pressure pulses would travel at lower velocities than lower velocity ones. Such is the case for the plastic waves in uniaxial stress experiments (Hopkinson bars) and the time rise increases with distance [41]. However, for uniaxial strain experiments, the Hugoniot P–V/V_0 curve is concave upwards [36] (on loading) even below the Hugoniot elastic limit, showing that the pressure dependence of velocity will not result in rise time increases. The rise times in single crystals with low defect densities give a good indication of the above effects. Quartz transducers indicate that rise times are usually 0.01 μs or lower for single crystals [16, 18 - 21]. Laser interferometer measurements [42] suggest that the rise times are even lower (about 10^{-3} μs). No experiments have been conducted, to the author's knowledge, on iron single crystals. For this reason, Δt_e has to be estimated on the basis of the response of other materials.

3.6 Dislocation dynamical effects

The elastic wave rise time has been attributed to dislocation effects by Gillis and Hoge [25]. Dislocations are held responsible for the pulse attenuation and yield point formation [2, 4, 6, 9 - 13]. Undoubtedly, dislocations will, if in sufficient concentration, affect the rise time of the wave. This has, indeed, been proven by Jones and Mote [16]. While annealed single crystals exhibited short rise times (~0.01 μs), predeformation increased this value considerably. The effect of dislocation concentration on the pulse rise would require experimentation to be quantified. The intrinsically generated time rise (Δt_e) and the one due to the existence of dislocations (Δt_l) are the probable causes for the time rises (~0.005 μs) observed by laser interferometry [36] in annealed single crystals. Since these effects cannot be experimentally separated, it will be assumed that $\Delta t_e + \Delta t_l = 0.005$ μs. It is considered, of course, that the material is fully annealed; this is, indeed, the case of Jones and Holland's [26] iron samples.

TABLE 4

Calculated and observed rise times of elastic precur wave

Average grain diameter (μm)	Rise times (μs)	
	Calculated (This model)	Observed (Jones and Holland [26
9	0.049 4	0.028
30	0.066 7	0.074
70.3	0.083 6	0.088

3.7 Comparison of model with Jones and Holland's [26] results

Among all rise times estimated or calculated in the preceding Sections, only Δt_a was considered as dependent upon grain size. Table 4 shows the total rise times, Δt, for grain sizes of 9, 30 and 70.3 μm. These rise times were obtained using eqn. (1) and values estimated or calculated in Sections 3.1 - 3.6.

At this point it is worth presenting the results of Jones and Holland [26], as well as succinctly describing their experimental techniques. Explosively generated plane shock waves were passed through disc-shaped specimens (diameter: 62 mm, thickness: 19.05 mm) having parallel faces. The wave penetrated into the disc along one of its faces; a quartz gage was placed in contact with the other face and produced, with the aid of appropriate transducers, a continuous stress–time profile of the elastic–plastic wave. A more detailed description of the experimental setup and technique is provided elsewhere [37]. Characteristically, the wave consisted of an elastic precursor followed by a trailing plastic front and phase-transition wave. The shock amplitude of the plane wave was about 22×10^3 N/mm^2. Prior to shocking, the iron discs (0.20% C, 0.85% Mn, 0.26% Si, 0.12% Cu and traces of other elements) were heat treated at temperatures between 885 and 1300 °C to yield the desired grain sizes. The average grain diameters ranged from 9.0 to 70.3 μm and no reference is made to texturing . Due to the annealing temperature one can infer that the grains were equiaxed. However, the possibility of recrystallization and grain growth textures cannot be discarded [38]. Among other parameters of the wave,

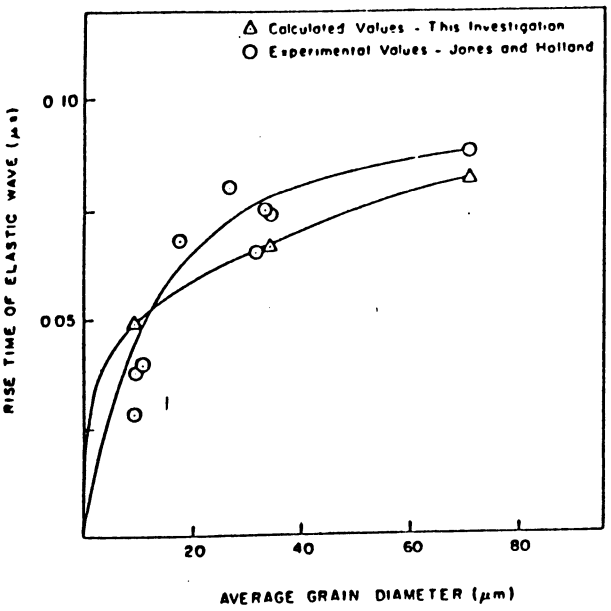

Fig. 8. Grain size dependence of rise time: comparison of results calculated from model with Jones and Holland's [26] results.

the elastic wave-front rise times were determined by Jones and Holland [26]. The rise times of the elastic waves were obtained from the stress–time plots, at the dynamic yield stress. This was defined by the intersection of extensions of straight lines coinciding with the leading elastic wave and the transition region preceding the slower platic wavefront, for the 9 μm condition. Whenever a yield point was formed (all other conditions) the peak was taken as the rise time. This rise time measures the interval between the instant when the first part of the wave reaches the quartz gage and the instant when the whole wave has reached it; at this moment the signal has reached its highest value for the elastic wave. The quartz gage has an active surface area orders of magnitude higher than the mean surface of the grains in contact with it. Hence, the rise time measured by it incorporates both the local rise time of the wave and the waviness due to different arrival times in different grains. So, it is the experimental parameter equivalent to Δt obtained from eqn. (1).

Jones and Holland's [26] rise times are also shown in Table 4 (they are listed in Table 4, p. 1042, of that reference), and it can be clearly seen that the agreement between calculated and experimental data is good. Figure 8 shows a graphic representation of the data. For simplicity, it is assumed that for infinitely small grain size, the material is isotropic and the wave retains its planarity and steepness of elastic front. It can be seen that the rise times increase with increasing grain size.

4. CONCLUSIONS

In spite of the fact that considerable effort has been devoted in the past towards understanding the attenuation and relaxation of the elastic precursor wave in shock loading experiments, its rise time has not been analyzed so thoroughly. This study shows that there are distinct differences in the rise times of different elastic waves, and that these differences appear to follow certain trends. The rise times of single crystals are substantially lower than polycrystals; they increase with transit distance inside the metal; in polycrystalline metals they are affected by grain size and texture.

A model for the elastic front is presented consistent with the rise time differences reported in the literature. The possible causes for the increase in actual rise time and generation of irregularities in the wave front were analyzed, and the following effects were considered: (a) anisotropy of wave velocity, (b) scattering by grain boundaries, (c) wave deflections at grain boundaries due to anisotropy of adjacent grains, (d) scattering due to mode conversion, (e) initial rise time of wave, and (f) dislocation dynamical effect. The different rise times were calculated or estimated, and a total rise time was obtained. The model was applied to the experimental conditions of Jones and Holland [26]. Calculations were made for three grain sizes, and it can be seen from Fig. 8 that a good agreement was obtained. Considering all the simplifying assumptions of the model and uncontrollable experimental variables (texture, quartz gage response, etc.), a satisfactory correlation was obtained. As the experiments, the model predicts increasing rise times with increasing grain size.

Although the calculations were not performed, the model shows qualitative agreement with the other results presented in the literature. It predicts much lower rise times for single crystals than for polycrystals, since

the terms Δt_a, Δt_b, Δt_c would vanish for the former ones. This is confirmed by the experimental measurements on single crystals [16 - 21, 36] and polycrystals [4, 16, 22 - 26]. If the texture of the material is pronounced, the term Δt_a would become reduced, because one of the orientation probabilities would dominate. Also, Δt_c would decrease, because the linearity of path would become more pronounced. Consequently, the rise time would be reduced; this is exactly what is reported by Stevens and Pope [23]. In their experiments on beryllium, the texture was varied without substantially affecting the grain size and shape. It is easy to show that Δt increases with propagating distance, corroborating Dick *et al.*'s [9] results, because the terms Δt_a - Δt_f are dependent upon penetration distance.

Finally, it is suggested that the proposed model can be applied, with the appropriate modifications, to surface ultrasonic waves in polycrystalline metals. It has been shown that both texture [39] and grain size [40] affect Raleigh waves in metals. The model herein presented could present a theoretical counterpart to the experiments (especially the effect of texture [39]).

ACKNOWLEDGEMENTS

The aid of Dr. R. W. Rohde, Sandia Laboratories, in providing the idea that initiated this work is gratefully acknowledged. Thanks are also due to Professor B. Palmer, South Dakota School of Mines and Technology, and Mr. Milton S. Carvalho, Military Institute of Engineering (Brazil), for assistance in computer programming. This work was supported in part by the Brazilian Army and FINEP.

REFERENCES

1 J. W. Taylor and M. H. Rice, J. Appl. Phys., 34 (1963) 364.
2 J. W. Taylor, J. Appl. Phys., 36 (1965) 3146.
3 W. G. Johnson and J. J. Gilman, J. Appl. Phys., 30 (1959) 129.
4 L. M. Barker, B. M. Butcher and C. H. Karnes, J. Appl. Phys., 37 (1966) 1989.
5 J. R. Holland, Acta Metall., 15 (1967) 691.
6 J. M. Kelly and P. P. Gillis, J. Appl. Phys., 38 (1967) 4044.
7 H. Conrad and H. Wiedersich, Acta Metall., 8 (1960) 128.
8 J. N. Johnson, J. Appl. Phys., 40 (1969) 2287.
9 R. W. Rohde, Acta Metall., 17 (1969) 353.
10 B. M. Butcher and D. E. Munson, in A. R. Rosenfield, G. T. Hahn, A. L. Bement, Jr. and R. I. Jaffee (eds.), Dislocation Dynamics, McGraw-Hill, New York, 1968, p. 591.
11 J. J. Gilman, Appl. Mech. Rev., 21 (1968) 767.
12 A. R. Rosenfield, G. T. Hahn, A. L. Bement, Jr. and R. I. Jaffee (eds.), Dislocation Dynamics, McGraw-Hill, New York, 1968.
13 W. Herrmann, D. L. Hicks and E. G. Young, in J. J. Burke and V. Weiss (eds.), Shock Waves and the Mechanical Properties of Metals, Syracuse Univ. Press, 1971, p. 23.
14 O. E. Jones, in R. W. Rohde, B. M. Butcher, J. R. Holland and C. H. Karnes (eds.), Metallurgical Effects at High Strain Rates, Plenum Press, New York, 1973, p. 33.
15 T. E. Arvidsson, Y. M. Gupta and G. E. Duvall, J. Appl. Phys., 46 (1975) 4474.
16 O. E. Jones and J. D. Mote, J. Appl. Phys., 40 (1969) 4920.
17 W. J. Murri and G. D. Anderson, J. Appl. Phys., 41 (1970) 3521.
18 Y. M. Gupta, G. E. Duvall and G. R. Fowles, J. Appl. Phys., 46 (1975) 532.
19 J. J. Dick, G. E. Duvall and J. E. Vorthman, J. Appl. Phys., 47 (1976) 3987.
20 L. E. Pope and A. L. Stevens, source cited in ref. 14, p. 349.
21 L. E. Pope and J. N. Johnson, J. Appl. Phys., 46 (1975) 720.
22 J. W. Taylor, source cited in ref. 12, p. 573.
23 A. L. Stevens and L. E. Pope, source cited in ref. 14, p. 459.
24 D. R. Grine, source cited in ref. 13, p. 367.
25 P. P. Gillis, K. G. Hoge and R. J. Wasley, J. Appl. Phys., 42 (1971) 2145.
26 O. E. Jones and J. R. Holland, Acta Metall., 16 (1968) 1037.
27 M. A. Meyers and M. S. Carvalho, Mater. Sci. Eng., 24 (1976) 131.
28 J. S. Rinehart, Stress Transients in Solids, Hyperdynamics, P. O. Box 392, Santa Fe, New Mexico, 1975, pp. 74, 83.
29 A. K. Ghatak and L. S. Kothari, An Introduction to Lattice Dynamics, Addison-Wesley, London, 1972, p. 70.
30 O. L. Anderson, in W. P. Mason (ed.), Physical Acoustics, Vol. IIIb, Academic Press, New York, 1965, p. 43.
31 H. Kolsky, Stress Waves in Solids, Dover, New York, 1963, p. 31.
32 N. L. Hickerson, in R. Kinslow (ed.), High-Velocity Impact Phenomena, Academic Press, New York, 1970, p. 23.
33 F. Borgnis, Phys. Rev., 98 (1955) 1000.
34 F. N. Rhines, K. R. Craig and R. T. DeHoff, Metall. Trans., 5 (1974) 413.
35 E. P. Papadakis, in W. P. Mason (ed.), Physical

Acoustics, Vol. IVb, Academic Press, New York, 1968, p. 269.
36 L. M. Barker and R. E. Hollenbach, J. Appl. Phys., 45 (1974) 4872.
37 R. A. Graham, F. W. Neilson and W. B. Benedick, J. Appl. Phys., 36 (1965) 1775.
38 G. C. Rauch, D. R. Thornburg and K. Foster, Metall. Trans. A, 8A (1977) 210.
39 B. R. Tittman and G. A. Alers, Metall. Trans., 3 (1972) 1307.
40 R. Kettler, R. Latiff and F. Fiore, Metall. Trans., 5 (1974) 952.
41 R. J. Wasley, Stress Wave Propagation in Solids, Marcel Dekker, New York, 1973, pp. 116, 213.
42 L. M. Barker and R. E. Hollenbach, J. Appl. Phys., 41 (1970) 4208.